LBL--31578

DE92 017119

Determination of Fe^{2+} and Fe^{3+} concentrations in semi-insulating InP:Fe

F.X. Zach, E.D. Bourret

Materials Sciences Division
Lawrence Berkeley Laboratory
University of California
Berkeley, California 94720

D. Bliss

USAF Rome Laboratory
Hanscom MA 01731-5000

E.R. Weber and E.E. Haller

Department of Materials Science and Mineral Engineering
University of California
Berkeley, CA 94720

January 1992

To be presented at the IEEE Meeting on Indium Phosphide and Related Materials, Newport, RI, April 20-24, 1992

This work was supported by the US Air Force under contract No. FQ 76190027, through the U.S. Department of Energy under Contract No. DE-AC03-76SF00098. One of the authors (FXZ) acknowledges financial support by the Deutsche Forschungsgemeinschaft.

MASTER

DISTRIBUTION OF THIS DOCUMENT IS UNLIMITED

Determination of Fe^{2+} and Fe^{3+} concentrations in semi-insulating InP:Fe

F.X. Zach[1], E.D. Bourret[1], D. Bliss[2], E. R. Weber[1,3], E.E. Haller[1,3]
[1] Lawrence Berkeley Laboratory, 1 Cyclotron Rd., Berkeley CA 94720, USA
[2] USAF Rome Laboratory, Hanscom MA 01731-5000 USA
[3] Department of Materials Science and Mineral Engineering, University of California, Berkeley CA 94720

Introduction

Semi-insulating InP is most commonly obtained by doping with the deep acceptor iron to compensate the shallow donors which otherwise render the material n-type conducting. As the Fermi level in semi-insulating InP is close to the iron acceptor level, both charge states - Fe^{2+} as well as Fe^{3+} corresponding to the acceptor level occupied/ unoccupied by an electron - are present. Meier et al. (1) presented a method based on absorption measurements in the nearbandgap region of InP to determine the concentration of both charge states separateley. In this paper we compare iron concentrations obtained by this method with the results from intracenter absorption, DLTS, EPR, Hall effect measurements and glow discharge mass spectroscopy. We present a new calibration for the optical absorption cross sections.

Experimental

Near infrared absorption measurements (NIRA) in the range 850 to 2000nm (1.45 eV to 0.62 eV) have been performed using a Cary 2390 UV-VIS-NIR spectrometer with the InP samples at liquid nitrogen temperature (77K). The absorption coefficient α was calculated from the experimental transmission values T:

$$T = (1-R)^2\exp(-\alpha d)/(1-R^2\exp(-2\alpha d)) .$$

This expression is valid for samples with two polished plane parallel surfaces and takes into account multiple reflections. Using the data for the refractive index as a function of photon energy from ref. (2) the reflection coefficient R could be determined. The absorption values between 1800 and 2000 nm (0.68 eV to 0.62 eV) where the absorption due to iron is neglegible, were used as the baseline of the absorption spectrum.

At a temperature of 6.5 K absorption measurements in the range of the Fe^{2+} intracenter absorption (appr. 2840 cm^{-1} or 0.35eV) were performed using a Digilab 80E-V vacuum fourier transform spectrometer with the sample mounted in an exchange gas optical cryostat.

A Bruker ER200D X-band spectrometer was used for the electron paramagnetic resonance (EPR) measurements. Absolute spin concentrations were determined from the doubly integrated spectra using a phosphorus doped silicon sample as a reference with the phosphorus concentration determined by Hall effect. Absolute calibrations were performed at a temperature and microwave power were the intensity of the Fe^{3+} EPR-signal follows the 1/T temperature dependence and the square root dependence on microwave power. For a comparison of different samples the temperature was set to the point where the maximum of the EPR-signal amplitude versus temperature dependence occurs. This way the effect of temperature fluctuations could be reduced.

Schottky diodes on n-type InP were prepared by either evaporating gold or electroplating cadmium (3) onto the samples. Before the metal deposition the surfaces were treated as outlined in ref. 3. Backside ohmic contacts were prepared using In-Sn eutectic prior to the processing steps necessary for the Schottky contacts. Net carrier concentrations were determined using capacitance versus voltage (C-V) and Hall effect measurements. For deep level transient spectroscopy measurements a standard setup with bias supply, pulse generator, Boonton capacitance bridge and a Miller correlator was used. Capacitance transients were recorded on a computer controlled digital oscilloscope. The emission rate was determined by fitting exponential curves to the experimental data. Very low emission rates were measured by applying a single voltage pulse and recording the subsequent transient on a x-t chart recorder. The capacitance transient following bias pulses of different amplitude were measured to evaluate the deep acceptor concentration and its depth profile.

Results

Near infrared absorption

Figure 1 shows the experimental near infrared absorption spectrum of a semi-insulating iron doped InP sample. The absorption is due to photo ionization transitions from the iron level. Two transitions contribute to this spectrum : photoexcitation of a hole from the empty acceptor level (Fe^{3+}) to the valence band with absorption cross section σ_p^o and excitation of an electron from the filled acceptor (Fe^{2+}) to the conduction band with absorption cross section σ_n^o. The cross sections for both processes have been determined in ref. (4) using photocapacitance. Included in the figure is a fit of the experimental spectrum using $\alpha(\lambda) = \sigma_n^o[Fe^{2+}] + \sigma_p^o[Fe^{3+}]$ with the concentrations of the two charge states as fitting parameters. A good fit of the spectrum can be obtained between 900 and 1500 nm (1.38 to 0.826 eV). The concentration of Fe^{3+} is mainly determined by the low absorption values at wavelengths around 1300 nm (0.95 eV) where the

cross section σ_n^0 is comparatively small. Uncertainties in the baseline strongly affect these concentrations. Both iron concentrations can also be calculated from the two linear equations :

$$\alpha(\lambda_1) = \sigma_n^0(\lambda_1)\,[Fe^{2+}] + \sigma_p^0(\lambda_1)\,[Fe^{3+}]$$

$$\alpha(\lambda_2) = \sigma_n^0(\lambda_2)\,[Fe^{2+}] + \sigma_p^0(\lambda_2)\,[Fe^{3+}]$$

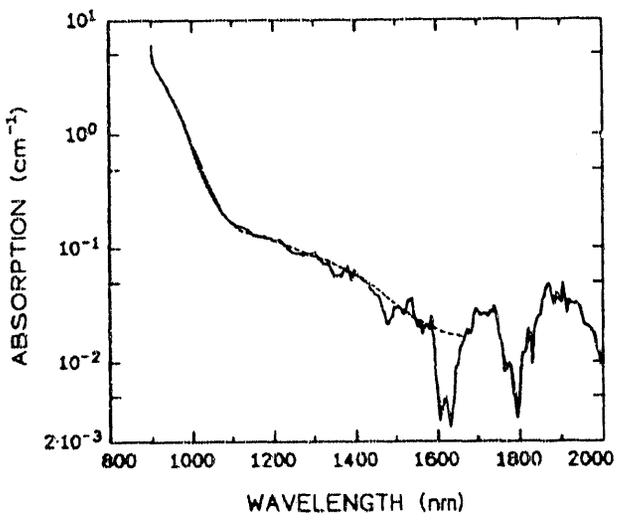

Figure 1 : Near bandgap absorption spectrum of a semi insulating InP:Fe sample at 77K. The figure shows the experimental spectrum together with a fit (points) using the absorption cross sections from ref. 4. The concentrations obtained from the fit are: $[Fe^{2+}] = 1.5\times10^{15}$ cm^{-3} and $[Fe^{3+}] = 1.7\times10^{15}$ cm^{-3}

Wavelengths of λ_1 = 970 and λ_2 = 1010 nm have been chosen for the calculation of the iron concentrations. The procedure outlined above essentially follows the one already demonstrated in ref. (1) for iron and ref.(5) for the similar case of EL2 in GaAs. Due to the fact that the absorption bands are very broad and featureless additional defects other than iron might contribute to the absorption as is suspected in ref. (6). We therefore compared the results obtained from the near infrared absorption (NIRA) with measurements that specifically detect one of the two charge states and allow quantitative measurements.

Intracenter absorption

Fe^{2+} shows characteristic absorption lines (7) due to intra center transitions between the crystal field split ^5E and $^5T_2$ states. At the temperature used for this measurement (6.5 K) only 2 out of the 4 possible lines are observed (see figure 2). The area underneath the absorption peaks has been used as a measure of the Fe^{2+} concentrations. In order to reduce the influence of small temperature variations, the area of both lines has been added including a weighing factor of 4/9 for the second line corresponding to the theoretical ratio of the absorption cross sections (See ref. 8). The absolute calibration of the absorption strength has been done using a n-type conducting sample whose iron concentration has been determined by DLTS. The DLTS- spectrum showed only one peak. The signature of this level, i.e. the electron emission rate as a function of temperature is plotted in figure 3 .

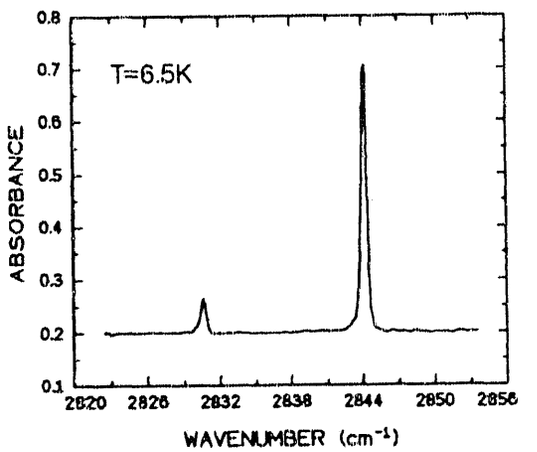

Figure 2: Optical absorption of InP:Fe in the region of the intra center transitions.

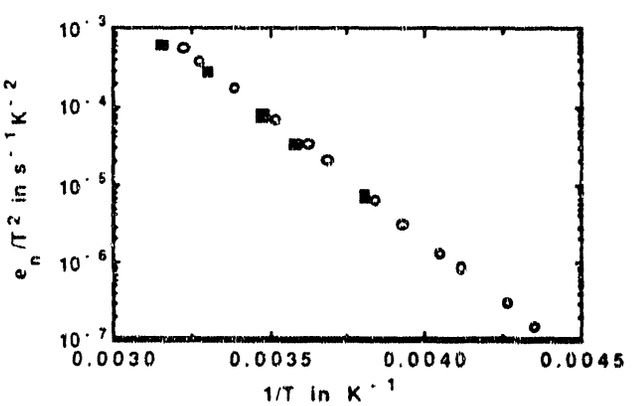

Figure 3 : Arrhenius plot of the electron emission rate divided by the square of the temperature as a function of 1/T. Open circles have been obtained in this work, filled squares are taken from ref.(9)

The experimental data agree very well with published values (9) for the iron deep level. An activation energy of 0.63 eV is determined from the plot. The net carrier concentrations determined by C-V and Hall measurements on this sample agree within 5 %. For a correct evaluation of the iron acceptor concentration and its depth profile from the experimental data an analytical model was used. This model provides an analytical expression for the trap concentration in terms of experimental parameters. In the case of small capacitance changes the result for the trap concentration reduces to the formula given in ref. (10). However it is also applicable to the case of large capacitance transients. Taking into account the additional corrections mentioned in ref. (11) the depth profile showed no indications of an inhomogeneous iron distribution. The iron concentration calculated

from this measurements agreed with an estimate based on the mobility of the sample at room temperature according to ref. (12).

EPR

For a quantitative measurement of Fe^{3+} concentrations the strength of its characteristic EPR-signal (7) has been used. Figure 4 shows the experimental spectrum with the magnetic field parallel to a <100> direction. The shape of the spectrum, consisting of 5 lines with the outer two not fully resolved, and its rotational pattern corresponds to the data reported in ref. (13). The doubly integrated spectra were used as a measure of the spin concentration.

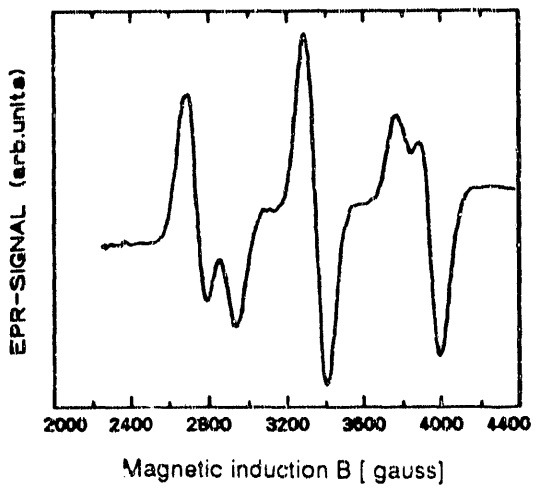

Figure 4 : EPR-spectrum of Fe-doped InP at T=30K. The microwave frequency is 9.41 GHz, the magnetic induction B is parallel to the <100> axis.

Comparison of results

In figures 5 and 6 we compare the iron concentrations obtained from an analysis of the near infrared absorption (NIRA) with the Fe^{2+} - concentrations as derived from the strength of the intra center absorption (FTIR) and the Fe^{3+} concentrations determined by EPR. If the NIRA is a reliable method for the determination of iron concentrations strictly linear relationships of the form $[Fe^{2+}]_{NIRA} = c_2\,[Fe^{2+}]_{FTIR}$ and $[Fe^{3+}]_{NIRA} = c_3\,[Fe^{3+}]_{EPR}$ are expected. The proportionality factors c should be equal to one if the absolute calibration of the NIRA is correct. The curves in both figures have been calculated using a least square fit. Two different points are discussed below: (i) deviations of the experimental curve from a linear relationship (ii) deviations of the proportionality factor from its ideal value 1.

(i) A fairly good fit of the experimental data is obtained for the $[Fe^{2+}]$ concentration (fig. 5). The optimized curve does show a small offset of about 0.5×10^{15} cm^{-3} $[Fe^{2+}]_{FTIR}$. Contributions to the absorption due to defects other than iron are especially important at low iron concentrations. It might be speculated that this is the reason for the offset of the calibration curve. However using a fit that allows no x-axis shift all the points lie within an error margin of about $\pm1\times10^{15}$ cm^{-3} $[Fe^{2+}]_{FTIR}$. This has to be compared with absolute values ranging from about 0.5 to 1×10^{16} cm^{-3} $[Fe^{2+}]_{FTIR}$.

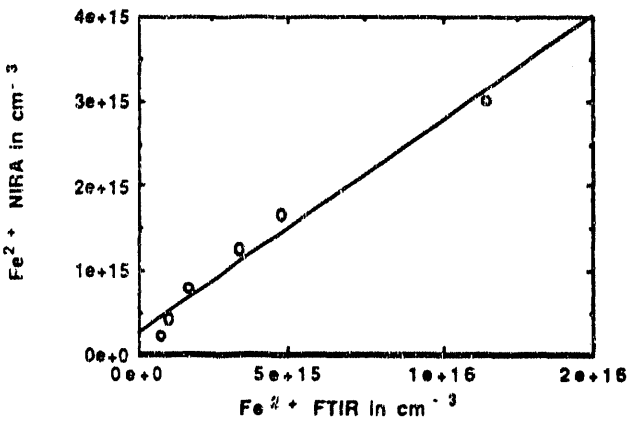

Figure 5 : Comparison of Fe^{2+} concentrations obtained from an analysis of the near bandgap absorption (NIRA) and the intra center absorption. The curve represents a least square fit of the form $[Fe^{2+}]_{NIRA} = 0.25\,[Fe^{2+}]_{FTIR} + 2.55\times10^{14}$ cm^{-3}

We now turn to a discussion of the Fe^{3+} concentrations. Again the experimental points are quite well described by a linear relationship. The deviations from a true linear relationship amount to less than $\pm1\times10^{16}$ cm^{-3} $[Fe^{3+}]_{EPR}$. This has to be compared with absolute values in the range about 0.5 to $2\times10^{17}cm^{-3}$ $[Fe^{3+}]_{EPR}$. The scattering of the experimental points in fig. 6 (Fe^{3+} concentrations) is not significantly larger than it is in fig. 5 (Fe^{2+} concentrations). This is partly due to the fact that a relativly short wavelength has been chosen for λ_2: At longer wavelengths the absorption is small and therefor strongly influenced by uncertainties in the exact baseline. This wavelength however mainly determines the Fe^{3+} concentrations due to the large ratio σ_p^0/σ_n^0 at long wavelengths according to ref. 4. The error margins above are obtained with αd values at 975 nm in the range 0.06 to 0.2 (d= thickness of the sample). We believe that under these conditions and with the uncertainties given above a reasonable assessment of the iron concentrations in semi-insulating InP: Fe can be obtained from NIRA-data. However it is not possible to exclude that for any given InP:Fe sample the effect of additional defect absorptions is within the errors given above. If such defects are present their effect is preferentially seen at low iron concentrations. In that case only EPR and measurements of the intra center absorption strength lead to unambiguous results.

(ii) For both, Fe^{2+} and Fe^{3+} concentrations, the proportionality factor c is significantly lower than 1

indicating that the absolute values of the absorption cross sections are too high. Similar conclusions have already been reached in refs. (1) and (14): In ref. (1) the total iron concentration $[Fe^{2+}] + [Fe^{3+}]$ determined from NIRA is compared to an estimated iron concentration. The estimate is based on the dopant concentration in the melt prior to the growth of the crystals. In ref. 14 the absorption of n and p-type samples, co-doped with iron has been measured. These values were compared to the iron content determined by atomic absorption spectroscopy (AAS).

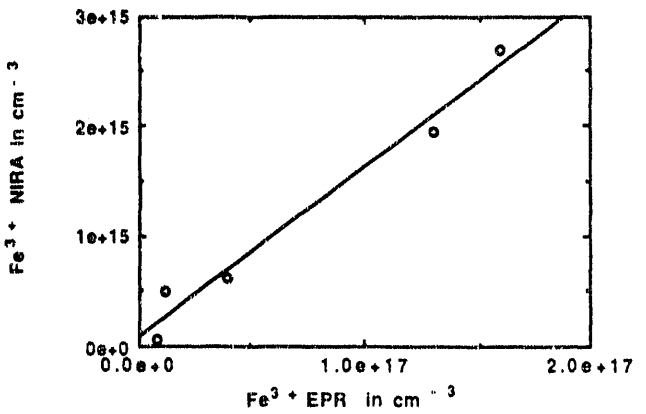

Figure 6 : Comparison of Fe^{3+} concentrations obtained from an analysis of the near bandgap absorption (NIRA) and EPR- measurements. The curve represents a least square fit of the form $[Fe^{3+}]_{NIRA} = 0.015\ [Fe^{3+}]_{EPR} + 8.0\times10^{13}\ cm^{-3}$

NIRA	Glowdischarge	EPR + FTIR
0.48	6	9.3
3.2	60	130
3.4	40	79

Table 1: Comparison of total iron concentrations determined by NIRA, Glow discharge mass spectroscopy and EPR and FTIR. All values are given in units of $10^{15}cm^{-3}$.

Our approach however seems more direct as EPR, DLTS, near infrared absorption and the intracenter absorption are only sensitive to $[Fe^{2+}]$ and/or $[Fe^{3+}]$. In both cases ($[Fe^{2+}]$, $[Fe^{3+}]$) the iron is sitting on its proper substitutional place. Techniques such as AAS or glow discharge mass spectroscopy however also measure iron that is located for example in precipitates. In table 1 we compare the data obtained by glow discharge mass spectroscopy with the data on the total electrically active iron concentrations as determined by NIRA and EPR / FTIR. In accordance to refs. 1 and 14 the concentrations determined by NIRA are at least an order of magnitude lower than the values from glow discharge. The values determined by EPR and FTIR however coincide within a factor of 2.

Based on our data for the concentrations of $[Fe^{2+}]$ and $[Fe^{3+}]$ the optical absorption cross sections can be recalibrated. The experimental absorption values at 975 nm are analyzed as a function of the $[Fe^{2+}]$ and $[Fe^{3+}]$ concentrations determined by FTIR and EPR respectivly. The absorption is described by :

$$\alpha(970nm) = \sigma_n^0(975nm)\ [Fe^{2+}] + \sigma_p^0(975\ nm)\ [Fe^{3+}]$$

The two dimensional fit of the experimental data results in the following absorption cross sections :

$$\sigma_n^0(975nm) = 1.2\times10^{-16}\ cm^2\ (T = 77K)$$

and $\sigma_p^0(975nm) = 7.0\times10^{-18}\ cm^2$ (T= 77K)

These values have to be compared with the ones given in ref. 4 which states $4.3\times10^{-16}\ cm^2$ for both cross sections. Ref. 14 gives $4.3\times10^{-17}\ cm^{-3}$ for different experimental conditions (λ=1000 nm, T = 300K).

We would like to thank G. Hofmann for providing the model to analyze the DLTS- depth profiles J. Heyman for assistance with the FTIR- spectrometer and P. Dreszer for assistance with the EPR spectrometer. One of the authors (FXZ) achnowledges financial support by the Deutsche Forschungsgemeinschaft. The use of the EPR, optical and electrical techniques at Lawrence Berkeley Laboratory supported by DOE is acknowledged. This work has been partially supported by the US Airforce under contract No. FQ 761910027.

---

(1) W. Meier, H. Ch. Alt, Th. Vetter, A. Winnacker; Semicond. Sci. Technol. Vol. 6, pp 297-300, 1991
(2) G.D. Pettit, W.J. Turner; J. Appl. Phys. Vol. 36, p. 2081, 1965
(3) C.J. Sa, L.G. Meiners; Appl. Phys. Lett. Vol. 46, pp. 1796-1798, 1986
(4) T. Takanohashi, K. Nakajima, J. Appl. Phys. Vol. 65, pp.3933-3936, 1989
(5) F.X. Zach, A. Winnacker; Japn. J. Appl. Phys. Vol. 28, p. 957-960, 1989
(6) A. Görger, J.M. Späth; Semicond. Sci. Technol., Vol. 6, pp. 800-806, 1991
(7) W.H. Koschel, U. Kaufmann, S.G. Bishop; Solid State Comm., Vol. 21, pp. 1069-1072, 1977
(8) K. Pressel, K. Thonke, A. Dörnen, G. Pensl; Phys. Rev. B , Vol. 43, pp. 2239-2245, 1991
(9) Landolt-Börnstein, Vol. III-22b, "Impurities and Defects in Group IV Elements and III-V Semiconductors", Springer-Verlag, 1989, p. 692
(10) ibid , p. 70
(11) D. Stievenard, D. Vuillaume: J. Appl. Phys. Vol. 60, pp. 973-979, 1986
(12) W. Walukiewicz, J. Lagowski, L. Jastrzebski, P. Rava, M. Lichtensteiger, C.H. Gatos, H.C. Gatos; J. Appl. Phys. Vol. 51, pp. 2659-2668, 1980
(13) G.K. Ippolitova, E.M. Omel'yanovskii,N.M. Pavlov, A.Ya. Nashel'skii, S.V. Yakobson ; Sov. Phys. Semicond., Vol. 7, pp. 773-777, 1977
(14) F. Mosel, A. Seidl, D. Hofmann, G. Müller; Appl. Surf. Sci., Vol.50, p. 364-368, 1991

END

DATE FILMED

9/4/92